IEEE Access
Multidisciplinary | Rapid Review | Open Access Journal

Received April 11, 2019, accepted May 25, 2019, date of publication May 30, 2019, date of current version June 17, 2019.

Digital Object Identifier 10.1109/ACCESS.2019.2920023

Investigation on the Material Failure in a Small Scale Automotive Camera Module via Root Cause Analysis and Experimental Validation

YONGJUN PAN, WEI DAI, AND YUE XIONG
School of Automotive Engineering, Chongqing University, Chongqing 400044, China

Corresponding author: Yongjun Pan (yongjun.pan@cqu.edu.cn)

This work was supported by the National Natural Science Foundation of China under Grant 11702039.

ABSTRACT Automotive camera modules are critical components for vision, detection, and recognition in an advanced driver assistance system. They usually consist of housing, a lens, a lens holder, a harness, seals, and printed circuit boards, which are assembled through screws, adhesive, and connectors. Due to a small and complex geometry of the components, the component material failure is a critical issue. In this paper, the lens holder material failure is investigated using the root cause analysis and experimental validation. First, a fishbone diagram model is created to analyze the potential causes and an action checklist is employed to identify the root cause. Second, the structure of the lens holder is optimized according to the finite-element analysis result. The numerical results show that the strength of the optimized lens holder is improved by nearly 35%. Finally, the torque test is carried out to validate the optimized structure experimentally. The presented analysis and validation procedure can be used to solve material failure issues for small-scale automotive components effectively.

INDEX TERMS Material failure, root cause analysis, fishbone diagram, experimental validation, automotive component.

I. INTRODUCTION

In recent years, special attention has been paid to the development of advanced driver assistance system (ADAS) since it can improve the active safety of the vehicles, for example lane departure warning [1], adaptive cruise control [2], blind spot detection [3], intelligent parking assistance [4], night vision [5]. Automotive camera modules, which are crucial electric components of ADAS, are able to satisfy the growing needs of automotive industry for front-view, rear-view and surround-view. Further, they can provide lens inspection, alignment, test and many other features required to deliver high-quality products to the automotive market. The global automotive camera module market is projected to grow dramatically in the future five to ten years. This is mainly attributed to the growing influence of new car assessment program with the increasing installation of ADAS in passenger cars and light commercial vehicles around the world. Due to its applications directly linked to the safety of passengers, it is critical to ensure the quality and reliability of the automotive camera module.

The design of automotive camera module has become a priority to improve the active safety and reliability of the vehicles. The material failure issue of camera module components is one of the most typical failure modes. A number of contributions related to the failure issues and fracture behaviors for automotive components have been reported recently. To predict fracture behaviors and the ultimate load-bearing ability of the fiber-reinforced polymer laminates used in automotive components, Yun *et al.* developed a progressive damage model to reflect the interaction between delamination and intralaminar crack [6]. Witek *et al.* performed the failure and stress analysis of the connecting rod of turbocharged diesel engine using advanced finite element method and experimental validation [7]. Jo *et al.* presented experimental and analytical results on deformation behavior of automotive gears under cyclic stress conditions including axial, torsional and combined axial-torsion loading [8]. Kalnaus *et al.* investigated the effect of inactive components of the electric vehicle battery module on mechanical response and failure of pouch

The associate editor coordinating the review of this manuscript and approving it for publication was Zhixiong Peter Li.

cells by out-of-plane indentation in a specially designed setup [9]. Chen *et al.* investigated mixed-mode fatigue crack growth behavior of an automotive adhesive bonding system using a compound compact mixed mode specimen [10]. Kong *et al.* established a multiple linear regression based spring durability models for predicting the fatigue life of automotive coil springs based on the vertical vibrations of the vehicle and natural frequencies of the vehicle suspension system [11]. These studies improve the strength of automotive components and the safety of vehicles. However, the investigation of material failure issues occurred in small scale automotive component such as camera module is rarely found in the literature. In this paper, the root cause analysis of a lens holder material failure is carried out using fishbone diagram model, finite element method and experimental validation.

II. COMPONENT STRUCTURE

Different types of automotive camera module structures are suited to different kinds of applications, and some are highly specialized to specific tasks. Various structures consists of several basic mechanical and electric components, namely a housing, a lens, a lens holder, seals, a harness and printed circuit boards (PCB). All components are connected and assembled using screws, adhesive and connectors. The structure of an automotive camera module used for intelligent parking assistance is described in Fig. 1.

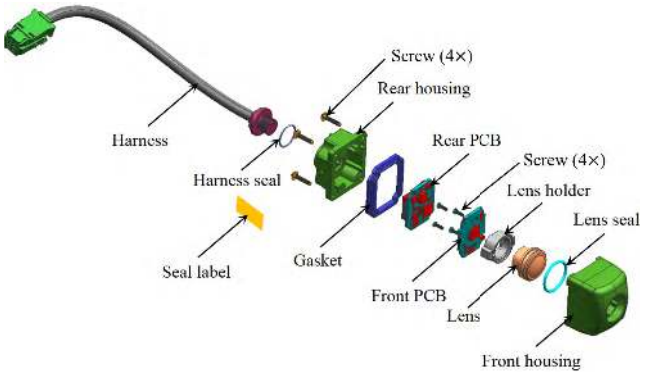

FIGURE 1. Exploded view of an automotive camera module.

As shown in Fig. 1, the front and rear housing are plastic components and connected by screws. The lens is designed to work well for automotive vision. The lens holder is a cylinder-shaped plastic component, having a helicoid ring which includes a male helicoid. It is located and fixed in the front PCB by locators and small screws. A stopper structure is also designed in the lens holder to prevent components of the lens barrel assembly, such as a flexible PCB, from interfering with the lens. The assembling of the lens, lens seal, lens holder and front PCB is described in Fig. 2.

The sub-assembly, in turn, is fixed to the ribs of the front housing by screws; whereas the lens inserts into the hole of the front housing. The ring-shaped lens seal is sandwiched

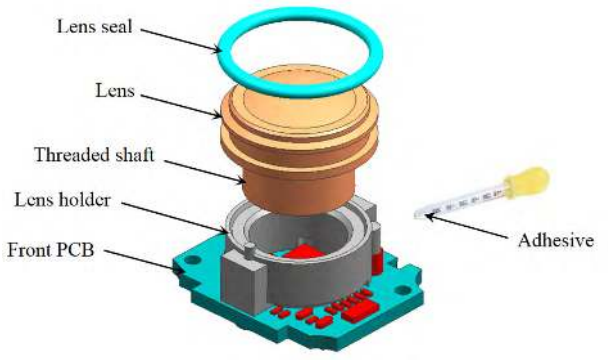

FIGURE 2. Assembling process of lens, lens holder, and front PCB.

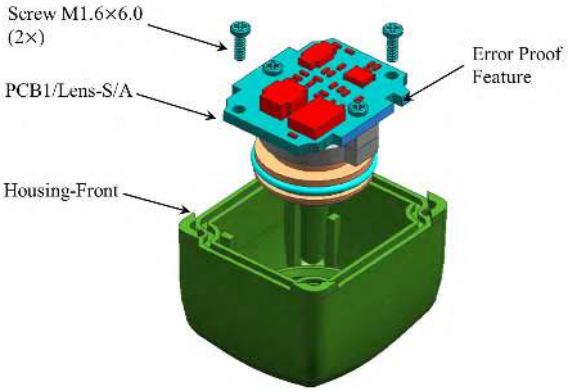

FIGURE 3. Assembling process of front PCB and front housing.

between the lens and front housing for sealing. This assembling process is described in Fig. 3. As can be seen from the figure, an error proof structure is provided to avoid incorrect assembly. The rear PCB is connected with the front PCB via a connector for information transmission and data exchange.

On the other hand, the harness is assembled to the rear housing, where a ring-shaped harness seal is used for water proofing. The front and rear housing is assembled using a gasket and screws for sealing and fixing. The assembly process is described in Fig. 4. After zoom lens calibration and lens distortion calibration, the automotive camera module can be equipped in various types of vehicles for intelligent parking assistance [12].

Due to small and complex geometry of the lens holder, it is difficult to avoid material failure issue during the design, manufacturing, logistics and assembling. The material failure always occurs in the lens holder as described in Fig. 5. In the design verification build process, 3 lens holders are cracked and 15 lens holders are found material failure during tear down (146 samples). The material failure process would be accelerated after high temperature test.

III. ROOT CAUSE ANALYSIS VIA FISHBONE DIAGRAM

The fishbone diagram, which is also known as the cause and effect diagram, was invented by Dr. Kaoru Ishikawa to

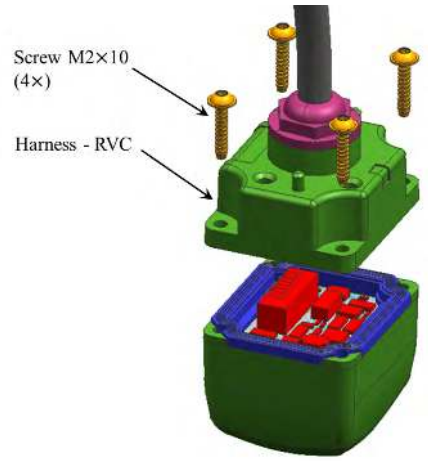

FIGURE 4. Assembling process of rear and front housing.

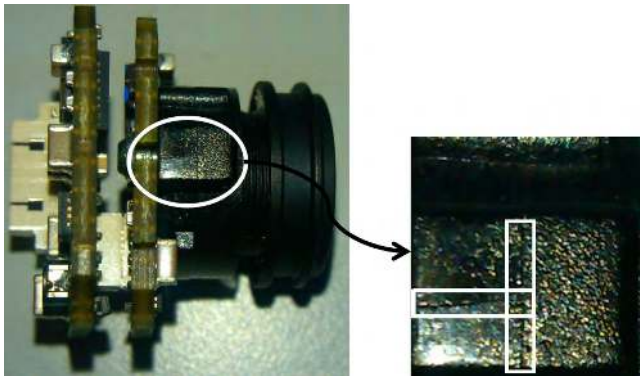

FIGURE 5. Lens holder material failure.

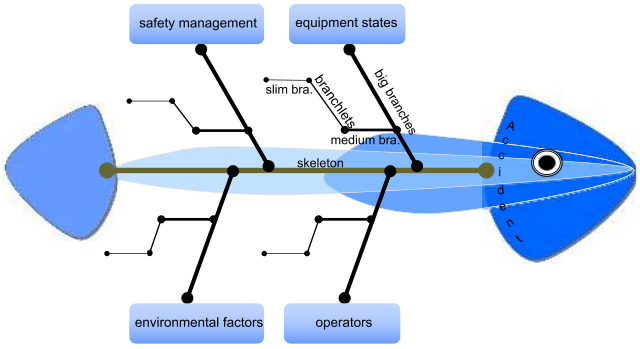

FIGURE 6. Structure of fishbone diagram model.

help engineers categorize the potential causes of a problem in order to find its root cause [13]. It collects potential causes through a graphic format that facilitates an organized approach to problem solving. It has been widely used in various fields to indicate the relationship between a problem and its underlying causes in an obvious way [14]–[18]. Fishbone diagram can systematize complicated potential causes with step by step in-depth study to identify the root cause [19]. The basic structure of fishbone diagram is described in Fig. 6.

When starting the lens holder material failure investigation, we first analyze the factors that contribute to the failure mode most, and then followed by departure from the big potential causes to find the middle, small and less ones, finally to detect and identify the root cause. The fishbone diagram model can be developed according to the following procedure [20], [21]:

1) Create a head to list the problem or issue to be investigated
2) Create a backbone for the fish (straight line leading to the head)
3) Identify at least four rough causes that may contribute to the issue. Connect them with arrows to the spine. The main bones of the fish are then created
4) Brainstorm around each rough cause to document potential causes that may contribute to the issue. Use 5 Whys or other questioning processes to keep the conversation focused [22]
5) Continue breaking down each potential cause until the root cause has been identified

The 5 Ms, which represents machine, method, material, man power and measurement, is one of the most common frameworks of root cause analysis for manufacturing issue. In recent years, the framework has been expanded to include mission & mother nature, management & money power and maintenance. This framework is referred to as the 8 Ms [23], [24]. If the issue is related with marketing, the 8 Ps framework can be used in the fishbone diagram. It consists of product, price, promotion, place, process, people, physical evidence and performance. The 4 Ss that consists of surroundings, suppliers, systems and skills is a typical framework for root cause analysis in service industry.

In this study, the failure issue is stated and confirmed, namely 2% lens holder samples cracked after assembly and 10% samples failure after tear down. The assembly process is to drive 2 screws into lens holder with 0.21 *Nm* torque through smart screw driver in production environment. This issue has closed relationship with structural design, manufacturing, logistics and assembling. Thus, the design, manufacture, logistics and assembly are identified as rough causes that may contribute to the material failure issue. These rough causes are classified and connected to the backbone of the fish as big branches. Brainstorming around big branches is carried out in the project team to collect potential root causes. Further, expert systems and lessons learned are used to help to analyze potential root causes [25]. Note that each big branch should be broken down as much as possible to identify the root cause clearly. The design and manufacturing related causes are the primary and secondary rough causes on the basis of lessons learned and team review. The fishbone diagram model, in turn, is created as described in Fig. 7 according to the above procedure.

To identify the root cause from the potential causes resulting from the fishbone diagram model, a checklist is generated to collect actions for the investigation and verification of the potential causes. The action checklist is described in Table 1. If one checks an action, the status of the corresponding

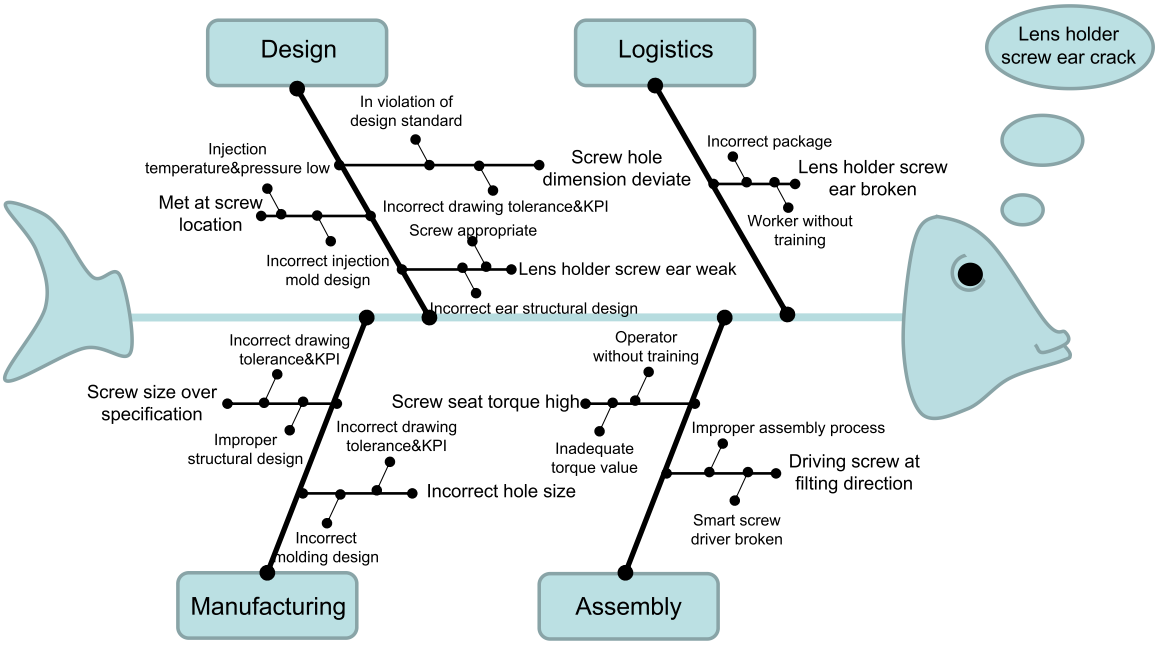

FIGURE 7. Structure of fishbone diagram model.

potential root cause will be decided. For example, the potential root cause that the screw hole dimension deviates design standard can be eliminated after checking the design standard. The status of this potential root cause, as a consequence, is defined to be closed. The root cause will be identified after completing the action checklist. The actions need the efforts of suppliers, process engineers and other team members of the project. It can be seen from Table 1 that the root cause of the material failure is the incorrect structural design of the lens holder component. The finite element method will be employed, in the next section, to verify the root cause and optimize the lens holder structure.

IV. STRESS ANALYSIS VIA FINITE ELEMENT METHOD

A. STRESS ANALYSIS

Finite element (FE) method can be used to simulate true physical systems (including geometry, constraints and loading conditions) through numerical approach to provide reliable and high-quality proposals [26], [27]. Further, it allows multiple what-if scenarios to be tested quickly and effectively and reduces the amount of prototype building and testing. It has therefore attracted much more attention in engineering design, manufacturing and assembly [28], [29].

Finite element analysis (FEA) has been widely used to predict and investigate crack formation issues in mechanical and electric engineering recently. To investigate the dynamic stress of the lens holder during assemble process, stress analysis of the lens holder based on the FE model was performed under boundary conditions. The governing equations of a FE model can be described as [30]:

$$\mathbf{M}\ddot{\mathbf{X}}(t) + \mathbf{C}\dot{\mathbf{X}}(t) + \mathbf{K}\mathbf{X}(t) = \mathbf{Q}(t) \tag{1}$$

where term $\mathbf{M}$ is the mass matrix of the FE model; terms $\mathbf{K}$ and $\mathbf{C}$ are the system damping matrix and stiffness matrix, respectively; vectors $\mathbf{X}(t)$ and $\mathbf{Q}(t)$ contain the displacements and applied loads in all nodes of the FE model, respectively.

These terms can be calculated as follows:

$$\mathbf{M} = \sum_e \int_{V_e} \rho \mathbf{N}^T \mathbf{N} dV \tag{2}$$

$$\mathbf{C} = \sum_e \int_{V_e} \mu \mathbf{N}^T \mathbf{N} dV \tag{3}$$

$$\mathbf{K} = \sum_e \int_{V_e} \mathbf{B}^T \mathbf{D} \mathbf{B} dV \tag{4}$$

$$\mathbf{Q} = \sum_e \int_{V_e} \mathbf{N}^T \mathbf{B} dV + \int_{s_\delta} \mathbf{N}^T \mathbf{P} ds \tag{5}$$

where terms ρ and μ are the density and damping coefficient of the component, respectively; term $\mathbf{N}$ contains the element shape functions; terms $\mathbf{B}$ and $\mathbf{D}$ are the strain-displacement matrix and elastic matrix of the FE model, respectively; term $\mathbf{P}$ contains the distributed external loads on the boundary s_δ.

The material of the lens holder is defined as PC+10%GF. The yield stress is close to 60 *MPa* (60 *MPa* is used in the FEA), and the density is 1.25 g/cm^3. The FE model is built up on the framework of Hypermesh as described in Fig. 8. A uniform pressure of 100 *MPa* is imposed to the lens holder ear. This is the pressure that the screw hole will experience during the screw formation. The stress contour of the lens holder ear, therefore, is obtained based on the FE model imposing external forces and boundary conditions, which is described in Fig. 9. Note that the symmetry FE model is employed to save CPU time. It can be seen that the hoop stresses near the

TABLE 1. Root cause analysis checklist.

Rough causes	Potential root causes	Actions	Status
Screw hole dimension deviation			
	In violation of design standard	Check with design standard	Closed
	Incorrect drawing tolerance& KPI	Check the 2D drawing	Closed
Met line at screw location			
	Improper injection mold design	Tooling supplier follows	Closed
	Low injection temperature&pressure	Product supplier follows	Closed
Lens holder ear weak			
	Incorrect ear structural design	Finite element analysis	**Open**
	Screw misuse	Check with process engineer	Closed
Screw size over specification			
	Incorrect drawing tolerance& KPI	Check the 2D drawing	Closed
	Improper structural design	Check the 3D data	Closed
Incorrect hole size			
	Incorrect drawing tolerance& KPI	Check the 2D drawing	Closed
	Incorrect molding design	Tooling supplier follows	Closed
Lens holder ear broken			
	Incorrect logistics	Check package and logistics	Closed
	Worker misoperation	Check at the plant	Closed
Screw seat torque high			
	Incorrect torque setup	Re-do torque study	Closed
	Operator without training	Check with process engineer	Closed
Driving screw at tilting direction			
	Incorrect assembling process	Check with process engineer	Closed
	Smart screw driver broken	Check at the plant	Closed

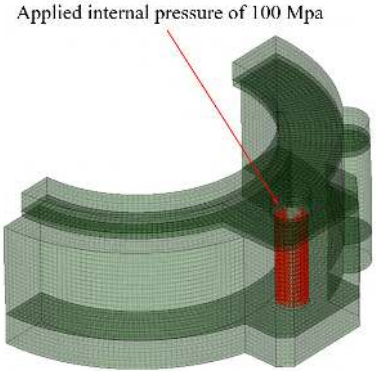

FIGURE 8. FEA model of lens holder.

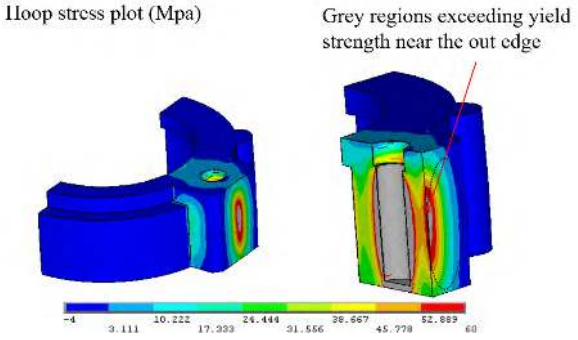

FIGURE 9. Stress contour of lens holder.

edge of the hole exceed the yield limit. If there is any weld line at this junction, the hole is likely to crack during the thread formation as the material strength degrades drastically. The root cause of the lens holder material failure is identified finally.

B. STRUCTURAL OPTIMIZATION

The solving approach for structural optimization mainly contains analytical and numerical methods. The application of structural optimization derived from analytical methods is extremely limited due to the complexity of the structures and materials and boundary conditions. Alternatively, numerical methods have been widely used to solve the structural

optimization problems. In recent years, with the theory development of topology optimization for complex continuum structures, the scale and speed of structural optimization are improved dramatically. Topology optimization can be incorporated in the early phase of the product development process to propose an optimized design [31]–[33]. Several methods have been introduced for topology optimization of complex continuum structures, such as the level set method, the evolutionary structural optimization method, the solid isotropic microstructure with penalization (SIMP) method and so on [34], [35].

SIMP method employed in this section is based on the continuous variables and elastic modulus of material. The topology optimization is, in turn, accomplished by removing the value of small variables. SIMP method can associate the density of design variables with the element elastic modulus by interpolation functions [36], [37]. The mathematical model for SIMP approach is described as:

$$E^P(x_e) = E^{min} + x_e^p(E^0 - E^{min}) \tag{6}$$

where E^P represents the elastic modulus after interpolation. Terms E^0 and E^{min} represent the elastic modulus of solid material part and void part, respectively. Material interpolation schemes regard the design variables as continuous variables between complete void and fill. The value x^{min} in Eq. 6 is a practical lower bound of the element density introduced to avoid singularity during the numerical implementation. An example is that the maximum strength of a structure is sought for a given amount of material under certain boundary conditions.

We define the design variable to be the thickness of the lens holder structure, and the design domain is 0 to 0.5 *mm* due to the limited space inside the camera module. The structural strength of the lens holder is the objective function. The boundary conditions and applied forces are the same with the previous finite element analysis. By taking into account the ease of manufacturing, the wall thickness near the edge of the screw hole has increased 0.4 *mm* to absorb hoop stress through the implementation of topology optimization. Note that the thickness increases only on left and right side. We hope this simple optimization can eliminate the crack issue. The optimized structure of the lens holder ear is described in Fig. 10.

The finite element method is carried out again for verification since the employed structure is not exactly the same with the optimized structure obtained by topology optimization method; further, the ease of manufacturing has been considered. The stress contour of the optimized lens holder ear is descried in Fig. 11. Some conclusions can be drawn according to the finite element analysis result:

1) The hoop stresses near the edge of the hole are well within the yield limit.
2) There is around 35% reduction of maximum stress in optimized structure.
3) The screw hole appears to be safe during the screw thread formation.

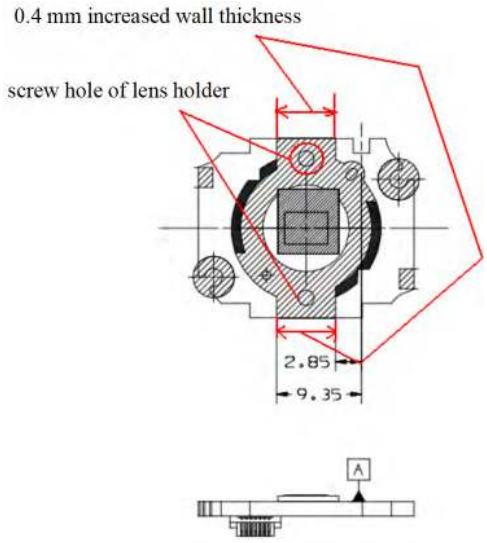

FIGURE 10. Optimized lens holder structure.

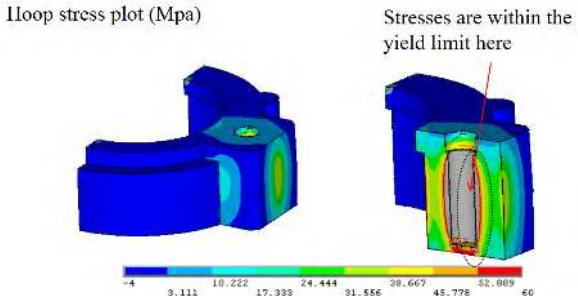

FIGURE 11. Stress contour of optimized lens holder.

V. EXPERIMENTAL VALIDATION

Finite element analysis does not simulate the real formation of threads in the hole, but instead an equivalent pressure is used and results would follow a similar trend. Experimental validation, in turn, is a critical part to validate the finite element analysis result [38]–[40]. In this section, driving screw test is performed to validate the numerical results of the recommended lens holder structural design.

The torque test is carried out with process engineers at the plant. The goal is to validate the optimized structure and determine the region where the screw seats and where the screw fails. A smart screw driver, a fixture, a torque study measurement device, 100 front PCB, 100 optimized lens holders and 200 screws are necessary for the torque test. The setup is described in Fig. 12. In many cases the smart screw driver may be larger than the actual production driver since the goal of the torque test is to drive the screw to its failure point. The torque test should emulate as close as possible the actual or intended production environment. Therefore it would be ideal to match the production driver setup, specifically rundown speed. If a multistage rundown strategy is used in production, it is recommended to use a single stage speed in torque test, and the torque test speed is equal to the

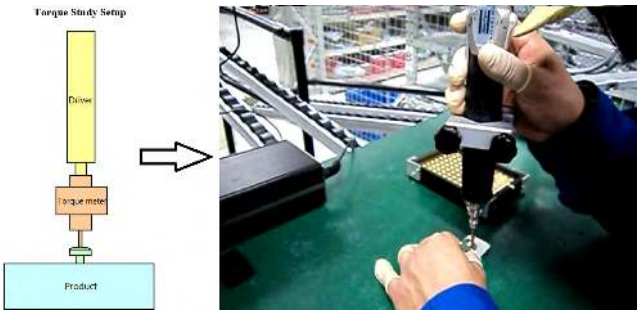

FIGURE 12. Torque test setup.

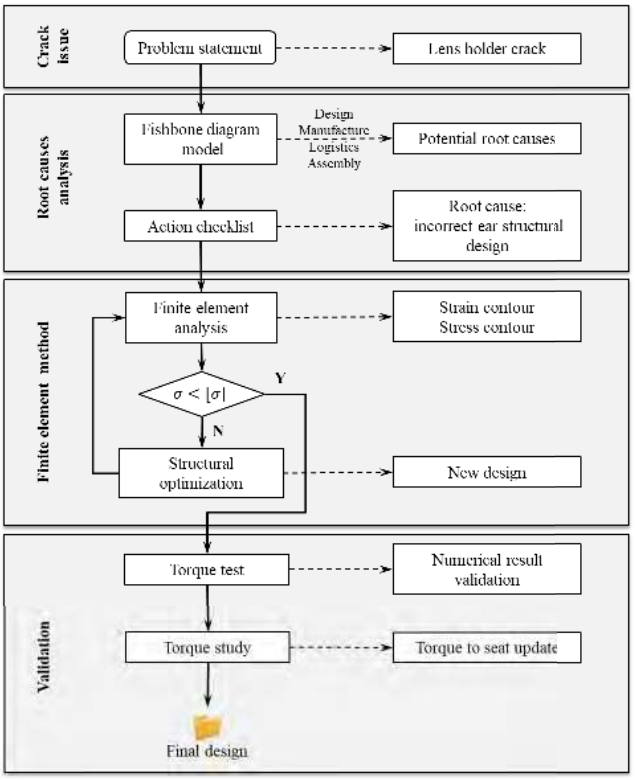

FIGURE 13. Fishbone diagram and finite element method based procedure.

final assembly speed used in production. The same assembly sequence should be emulated in the torque test if a specific assembly sequence will be followed in production.

100 samples are assembled according to production driver setup, 30 of which are used for torque study. Test results show no crack issue observed in the optimized lens holder. Further, no samples with material failure are found after high temperature test and tear down. The material failure issue is completely eliminated by applying the optimized lens holder design. The fishbone diagram and finite element method based procedure for the root cause analysis can be illustrated in Fig. 13.

On the other hand, 30 sets of torque data are collected from the torque study to update the production driver parameters. The fail torque and seat torque for the new lens holder

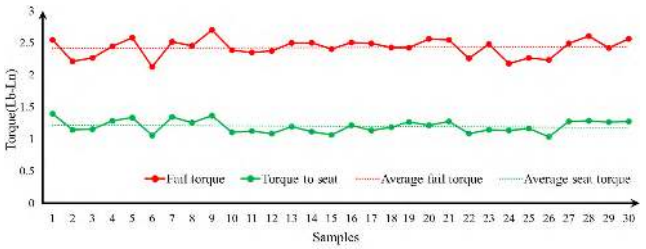

FIGURE 14. Fail torque and seat torque.

assembling are described in Fig. 14. It can be calculated that the average fail toque (T_f) and seat torque (T_s) are 2.42 and 1.19 lb-in, respectively. Note that the torque study should be conducted again if the screw hole and related features change.

VI. CONCLUSION

This paper established an effective procedure of material failure investigation for a small scale automotive camera module by employing root cause analysis and experimental validation. The procedure, which consists of problem statement, root cause analysis, finite element analysis and experimental validation, involves multidisciplinary approaches that can be used for full consideration of failure mode. The potential root causes are collected and investigated through a quality improvement tool fishbone diagram. The root cause is identified after completing an action checklist corresponding to all potential causes. In the problem solving phase, the lens holder structure is optimized according to the finite element analysis results, the new structure shows 35% improvement in structural strength. The torque test is carried out to validate the numerical simulation result. The fail torque and seat torque is re-defined based on the torque study to update the production driver parameters. Overall, a simple yet analysis and verification procedure has been presented to identify the root cause of a lens holder material failure issue. Those small scale automotive components whose failure modes are difficult to identify can benefit from the procedure.

REFERENCES

[1] J. Navarro, J. Deniel, E. Yousfi, C. Jallais, M. Bueno, and A. Fort, "Influence of lane departure warnings onset and reliability on car drivers' behaviors," *Appl. Ergonom.*, vol. 59, pp. 123–131, Mar. 2017.
[2] A. Weißmann, D. Görges, and X. Lin, "Energy-optimal adaptive cruise control combining model predictive control and dynamic programming," *Control Eng. Pract.*, vol. 72, pp. 125–137, Mar. 2018.
[3] M. Ra, H. G. Jung, J. K. Suhr, and W.-Y. Kim, "Part-based vehicle detection in side-rectilinear images for blind-spot detection," *Expert Syst. Appl.*, vol. 101, pp. 116–128, Jul. 2018.
[4] M. Heimberger, J. Horgan, C. Hughes, J. McDonald, and S. Yogamani, "Computer vision in automated parking systems: Design, implementation and challenges," *Image Vis. Comput.*, vol. 68, pp. 88–101, Dec. 2017.
[5] C. Fu, R. Duan, and E. Kayacan, "Visual tracking with online structural similarity-based weighted multiple instance learning," *Inf. Sci.*, vol. 481, pp. 292–310, May 2019.
[6] K. Yun, S. Kwak, Z. Wang, M. Chang, J. Kim, J. Liu, and C. Ri, "A damage model reflecting the interaction between delamination and intralaminar crack for failure analysis of FRP laminates," *Appl. Sci.*, vol. 9, no. 2, p. 314, 2019.

[7] L. Witek and P. Zelek, "Stress and failure analysis of the connecting rod of diesel engine," *Eng. Failure Anal.*, vol. 97, pp. 374–382, Mar. 2019.

[8] B. Jo, S. Sharifimehr, Y. Shim, and A. Fatemi, "Cyclic deformation and fatigue behavior of carburized automotive gear steel and predictions including multiaxial stress states," *Int. J. Fatigue*, vol. 100, pp. 454–465, Jul. 2017.

[9] S. Kalnaus, H. Wang, T. R. Watkins, A. Kumar, S. Simunovic, J. A. Turner, and P. Gorney, "Effect of packaging and cooling plates on mechanical response and failure characteristics of automotive Li-ion battery modules," *J. Power Sources*, vol. 403, pp. 20–26, Nov. 2018.

[10] Q. Chen, H. Guo, K. Avery, H. Kang, and X. Su, "Mixed-mode fatigue crack growth and life prediction of an automotive adhesive bonding system," *Eng. Fracture Mech.*, vol. 189, pp. 439–450, Feb. 2018.

[11] Y. S. Kong, S. Abdullah, D. Schramm, M. Z. Omar, and S. M. Haris, "Development of multiple linear regression-based models for fatigue life evaluation of automotive coil springs," *Mech. Syst. Signal Process.*, vol. 118, pp. 675–695, Mar. 2019.

[12] M. Pereira, D. Silva, V. Santos, and P. Dias, "Self calibration of multiple LIDARs and cameras on autonomous vehicles," *Robot. Auton. Syst.*, vol. 83, pp. 326–337, Sep. 2016.

[13] G. Ilie and C. N. Ciocoiu, "Application of fishbone diagram to determine the risk of an event with multiple causes," *Manage. Res. Pract.*, vol. 2, no. 1, pp. 1–20, 2010.

[14] J. I. Chang and C.-C. Lin, "A study of storage tank accidents," *J. Loss Prevention Process Ind.*, vol. 19, no. 1, pp. 51–59, 2006.

[15] A. Bouras, "Quality tools to improve the communication level in the surgery department at a local hospital," *Comput. Hum. Behav.*, vol. 51, pp. 843–851, Oct. 2015.

[16] K. Ramachandran, K. Kadirgama, O. I. Awad, D. Ramasamy, M. Samykano, and W. H. Azmi, "Comprehensive review of principle factors for thermal conductivity and dynamic viscosity enhancement in thermal transport applications: An analytical tool approach," *Int. Commun. Heat Mass Transf.*, vol. 98, pp. 13–21, Nov. 2018.

[17] Z. Xu, Y. Dang, and P. Munro, "Knowledge-driven intelligent quality problem-solving system in the automotive industry," *Adv. Eng. Inform.*, vol. 38, pp. 441–457, Oct. 2018.

[18] L. Berman, M. V. Raval, and A. Goldin, "Process improvement strategies: Designing and implementing quality improvement research," *Seminars Pediatric Surg.*, vol. 27, no. 6, pp. 379–385, 2018.

[19] M. A. Alam, D. Das, M. H. Azarian, B. Sood, and M. G. Pecht, "Influence of molding compound on leakage current in MOS transistors," *IEEE Trans. Compon., Packag., Manuf. Technol.*, vol. 1, no. 7, pp. 1054–1063, Jul. 2011.

[20] T. Luo, C. Wu, and L. Duan, "Fishbone diagram and risk matrix analysis method and its application in safety assessment of natural gas spherical tank," *J. Cleaner Prod.*, vol. 174, pp. 296–304, Feb. 2018.

[21] J. Romero, M. H. Azarian, C. Morillo, and M. Pecht, "Effects of moisture and temperature on membrane switches in laptop keyboards," *IEEE Trans. Device Mater. Rel.*, vol. 18, no. 4, pp. 535–545, Dec. 2018.

[22] S. J. Benjamin, M. S. Marathamuthu, and U. Murugaiah, "The use of 5-WHYs technique to eliminate OEE's speed loss in a manufacturing firm," *J. Qual. Maintenance Eng.*, vol. 21, no. 4, pp. 419–435, 2015.

[23] G. Watson, "The legacy of Ishikawa," *Qual. Prog.*, vol. 37, no. 4, pp. 54–67, 2004.

[24] B. G. Dale, T. van der Wiele, and J. van Iwaarden, *Managing Quality*. Hoboken, NJ, USA: Wiley, 2007.

[25] C. Zhu, J. Zhu, L. Wang, and M. S. Mannan, "Lessons learned from analyzing a VCE accident at a chemical plant," *J. Loss Prevention Process Ind.*, vol. 50, pp. 397–402, Nov. 2017.

[26] T. J. R. Hughes, *The Finite Element Method: Linear Static and Dynamic Finite Element Analysis*. Upper Saddle River, NJ, USA: Prentice-Hall, 2000.

[27] Z. Li, Y. Jiang, C. Hu, and Z. Peng, "Difference equation based empirical mode decomposition with application to separation enhancement of multi-fault vibration signals," *J. Difference Equ. Appl.*, vol. 23, nos. 1–2, pp. 457–467, Feb. 2017.

[28] G. Zhang, Y. Zhang, X. Fu, and X. Zhang, "Effects of daily mastication on bone remodeling with implant-tooth-supported fixed partial prosthesis: A finite element study," *IEEE Access*, vol. 7, pp. 33851–33858, 2019.

[29] A. V. Tran, X. Zhang, and B. Zhu, "Effects of temperature and residual stresses on the output characteristics of a piezoresistive pressure sensor," *IEEE Access*, vol. 7, pp. 27668–27676, 2019.

[30] O. Zienkiewicz, R. Taylor, and D. Fox, *The Finite Element Method for Solid and Structural Mechanics*. Amsterdam, The Netherlands: Elsevier, 2014.

[31] L. Xia and P. Breitkopf, "Recent advances on topology optimization of multiscale nonlinear structures," *Arch. Comput. Methods Eng.*, vol. 24, no. 2, pp. 227–249, 2017.

[32] L. Xia, L. Zhang, Q. Xia, and T. Shi, "Stress-based topology optimization using bi-directional evolutionary structural optimization method," *Comput. Methods Appl. Mech. Eng.*, vol. 333, pp. 356–370, May 2018.

[33] X. Tian, Q. Wang, G. Liu, Y. Liu, Y. Xie, and W. Deng, "Topology optimization design for offshore platform jacket structure," *Appl. Ocean Res.*, vol. 84, pp. 38–50, Mar. 2019.

[34] M. Burchill and M. Heller, "Optimal free-form shapes for holes in flat plates under uniaxial and biaxial loading," *J. Strain Anal. Eng. Des.*, vol. 39, no. 6, pp. 595–614, 2004.

[35] G. I. N. Rozvany, "A critical review of established methods of structural topology optimization," *Struct. Multidiscipl. Optim.*, vol. 37, no. 3, pp. 217–237, 2009.

[36] L. Xia, Q. Xia, X. Huang, and Y. M. Xie, "Bi-directional evolutionary structural optimization on advanced structures and materials: A comprehensive review," *Arch. Comput. Methods Eng.*, vol. 25, no. 2, pp. 437–478, 2018.

[37] Y. Zhang, M. Xiao, H. Li, L. Gao, and S. Chu, "Multiscale concurrent topology optimization for cellular structures with multiple microstructures based on ordered simp interpolation," *Comput. Mater. Sci.*, vol. 155, pp. 74–91, Dec. 2018.

[38] W. Kilpatrick, D. Brown, and A. G. Leacock, "The finite element implementation, validation and verification of a plane stress yield criterion for use in sheet metal forming analysis," *Int. J. Mech. Sci.*, vols. 101–102, pp. 363–375, Oct. 2015.

[39] Z. Li, D. Wu, C. Hu, and J. Terpenny, "An ensemble learning-based prognostic approach with degradation-dependent weights for remaining useful life prediction," *Rel. Eng. Syst. Saf.*, vol. 184, pp. 110–122, Dec. 2019.

[40] S. Dondapati, M. Trivedi, R. S. Dondapati, and D. Chandra, "Investigation on the mechanical stresses in a muffler mounting bracket using root cause failure analysis (RCFA), finite element analysis and experimental validation," *Eng. Failure Anal.*, vol. 81, pp. 145–154, Nov. 2017.